

# The Dahuiyeh (Zarand) earthquake of 2005 February 22 in central Iran: reactivation of an intramountain reverse fault

M. Talebian,<sup>1</sup> J. Biggs,<sup>3</sup> M. Bolourchi,<sup>1</sup> A. Copley,<sup>2</sup> A. Ghassemi,<sup>1</sup> M. Ghorashi,<sup>1</sup> J. Hollingsworth,<sup>2</sup> J. Jackson,<sup>2</sup> E. Nissen,<sup>3</sup> B. Oveisi,<sup>1</sup> B. Parsons,<sup>3</sup> K. Priestley<sup>2</sup> and A. Saiidi<sup>1</sup>

<sup>1</sup>Geological Survey of Iran, PO Box 13185-1494, Tehran, Iran

<sup>2</sup>COMET, Bullard Laboratories, Madingley Road, Cambridge, CB3 0EZ, UK. E-mail: jackson@esc.cam.ac.uk

<sup>3</sup>COMET, Department of Earth Sciences, Parks Road, Oxford, OX1 3PR, UK

Accepted 2005 October 10. Received 2005 October 6; in original form 2005 July 14

## SUMMARY

We used seismic body waves, radar interferometry and field investigation to examine the source processes of the destructive earthquake of 2005 February 22 near Zarand, in south–central Iran. The earthquake ruptured an intramountain reverse fault, striking E–W and dipping north at  $\sim 60^\circ$  to a depth of about 10 km. It produced a series of coseismic scarps with up to 1 m vertical displacement over a total distance of  $\sim 13$  km, continuous for 7 km. The line of the coseismic ruptures followed a known geological fault of unknown, but probably pre-Late Cenozoic, age and involved bedding-plane slip where the scarps were continuous at the surface. However, any signs of earlier coseismic ruptures along this fault had been obliterated by the time of the 2005 earthquake, probably by land sliding and weathering, so that the fault could not reasonably have been identified as active beforehand. The 2005 fault is at an oblique angle to the range-bounding Kuh Banan strike-slip fault, and may represent a splay from that fault, related to its southern termination. Other intramountain reverse faulting earthquakes have occurred in Iran, but this is the first to have produced a clear, mapped surface rupture, and to have been studied with InSAR. Faults of this type represent a serious seismic hazard in Iran and are difficult to assess, because their geomorphological expression is much less clear than the range-bounding reverse faults, which are more common and have been better studied.

**Key words:** active tectonics, earthquake source parameters, faulting, Iran, radar interferometry, seismology.

## 1 INTRODUCTION

On 2005 February 22 an earthquake of  $M_w$  6.4 struck a region of south–central Iran near Zarand, about 60 km north of the city of Kerman, the provincial capital (Fig. 1). The earthquake occurred at 05:55 am local time, in winter, so many people were indoors, and casualties were high in the villages affected, with approximately 500 killed in Dahuiyeh and Hotkan (Fig. 2). This paper is concerned with the coseismic faulting in the earthquake, and its tectonic and seismic hazard implications. These are interesting, for two main reasons.

First, this earthquake is the most recent in a series of destructive earthquakes in Kerman province (Table 1), starting with one of  $M_w$  5.8 in 1977 less than 30 km from the 2005 Dahuiyeh epicentre. The series continued with substantial earthquakes in 1981 ( $M_w$  6.6, 7.2) and 1998 ( $M_w$  6.6) SE of Kerman on the Gowk fault system (Berberian *et al.* 1984, 2001), followed by the devastating earthquake ( $M_w$  6.3) at Bam in 2003 (Talebian *et al.* 2004), about 280 km SE of the 2005 Dahuiyeh earthquake discussed here. The sys-

tem of faults responsible for these earlier earthquakes is a roughly N–S to NW–SE striking zone of right-lateral strike-slip faults that probably accommodates  $<5$  mm yr<sup>-1</sup> of right-lateral shear between central Iran and the Lut desert (Fig. 1; see Walker & Jackson 2002, 2004). For reasons that are not clear, it appears that this fault system is going through a period of substantial seismic activity; much more so than the equivalent N–S right-lateral strike-slip system on the east side of the Lut, which accommodates a faster ( $\sim 10$ – $15$  mm yr<sup>-1</sup>) shear between the Lut and Afghanistan (Walker & Jackson 2004), yet which has had relatively few earthquakes over the last 100 yr. Iran has a long-documented historical record of earthquakes, and apparent episodic bursts of activity in the fault zones bounding the relatively rigid desert interior has been noticed before (Ambraseys & Melville 1982; Berberian & Yeats 1999). The implications for major cities, such as Kerman, within these zones, are substantial.

Second, the 2005 Dahuiyeh earthquake involved reverse faulting, unlike the strike-slip faulting responsible for the earlier recent earthquakes in this zone mentioned above. Reverse-faulting earthquakes

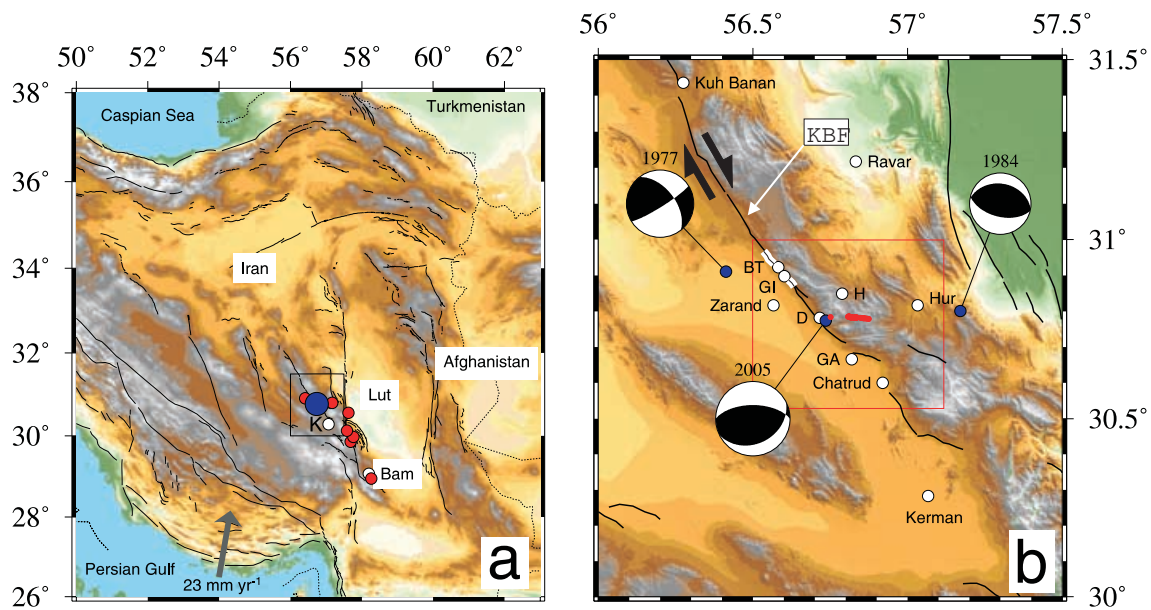


**Figure 1.** (a) Location map of Iran. The 2005 Dahuiyeh earthquake epicentre is marked by a large blue circle. Red circles are other earthquakes of  $M_w \geq 5.3$  on the fault system bounding the west side of the Lut desert since 1977 (see Table 1), discussed in the text. Solid lines are active faults. The box outlines the area in Fig. 1(b), and K is Kerman. The arrow at the bottom is the convergence direction between Arabia and Eurasia at this longitude (Vernant *et al.* 2004). (b) Detailed map of the Zarand region. Focal mechanisms are for earthquakes in Table 1; blue circles are their instrumental epicentres. Solid black lines are active faults, and the thick red line is the continuous part of the 2005 coseismic surface ruptures. The red box outlines the area in Fig. 6. KBF is the Kuh Banan Fault, BT is Bob Tangol, GI is Gisk, D is Dahuiyeh, H is Hotkan and GA is Gorchuiyeh. Topography is from the SRTM 90 m database. The white line running from north of BT to south of GI is the section of the KBF that ruptured in 1977.

are common in central and eastern Iran, and several devastating ones have occurred in modern times, such as the 1968 Ferdows, 1978 Tabas, 1994 Sefidabeh and 2004 Changureh earthquakes. All of these involved blind reverse faults along the edge of range fronts bordering the desert, and have surface geomorphological expressions that are clear (Walker *et al.* 2003, 2005; Berberian *et al.* 2000), even if they were not recognized at the time. By contrast, the reverse fault responsible for the 2005 Dahuiyeh earthquake was within a mountainous region, not along its edge, and at a high angle to the range front. Its location, and its identification for seismic hazard estimation, are far less obvious than for range-bounding faults. Its tectonic significance, and its implications for hazard assessment, both require serious attention.

## 2 TECTONIC AND GEOLOGICAL SETTING

The most striking geomorphological feature of the general epicentral region is the NW–SE range front forming a well-defined abrupt NE edge to the Zarand plain (Figs 1 and 2). This edge is defined by the Kuh Banan fault, which separates deformed Palaeozoic and Mesozoic sediments in the mountainous region to the east from the flat alluvial plain of Zarand. The Kuh Banan fault can be seen to dip east in the region of Bob-Tangol (Fig. 1) and has a reverse (or thrust) component to its displacement, which must be responsible for its associated topography. However, its most recent sense of motion seems to have been largely strike-slip, seen in the focal mechanism of the 1977 December 19 Bob-Tangol (or Gisk) earthquake (Fig. 1b, Table 1), which ruptured between 10 and 20 km of the Kuh Banan fault trace north of Zarand (Fig. 1b, Berberian *et al.* 1979; Ambraseys & Melville 1982). Our field observations of clear right-lateral offsets of Late Quaternary drainage systems near Gisk,

and a clear fault trace across an embayment south of Gisk, near  $30^{\circ}49'N$   $56^{\circ}40'E$ , which has very little associated topography, also attest to recent strike-slip motion with little reverse component.

The Kuh Banan fault becomes less distinct south of  $30^{\circ}45'N$ , where it seems to bend to the east to join a series of E–W scarps near Gorchuiyeh ( $30^{\circ}41'N$   $56^{\circ}49'E$ ) that are clearly the remnants of reverse-fault ruptures, upthrown to the north (Fig. 1). Young fault scarps with a NW–SE trend, upthrown to the NE, are seen again south of Chatrud, considerably closer to Kerman.

The 2005 Dahuiyeh earthquake did not rupture the Kuh Banan fault, but occurred on an E–W reverse fault within the mountainous region to the east (Fig. 2). As we show below, it had a northward dip of  $60^{\circ}$ – $65^{\circ}$ , which is steep even for reverse faults. Its epicentre is about 10–15 km west of an earlier, smaller ( $M_w$  5.3) earthquake on 1984 August 6 that damaged the village of Hur (Fig. 1b) and which also had a reverse-fault mechanism. In the east of this 1984–2005 epicentral region the rocks consist mostly of Triassic–Jurassic sediments, principally shales, sandstones and some limestones. In the west, adjacent to the Kuh Banan range front, the sediments are of Cambrian to Devonian age, dominated by sandstones, with some evaporite-rich units.

## 3 EARTHQUAKE SOURCE PARAMETERS

### 3.1 Data sources

An aim of this paper is to present what is known of the source parameters of the 2005 earthquake. We have three principal sources of information, from teleseismic seismology, coseismic ruptures observed at the surface, and radar interferometry (InSAR). Together, they form a coherent picture of the general features of the coseismic faulting.

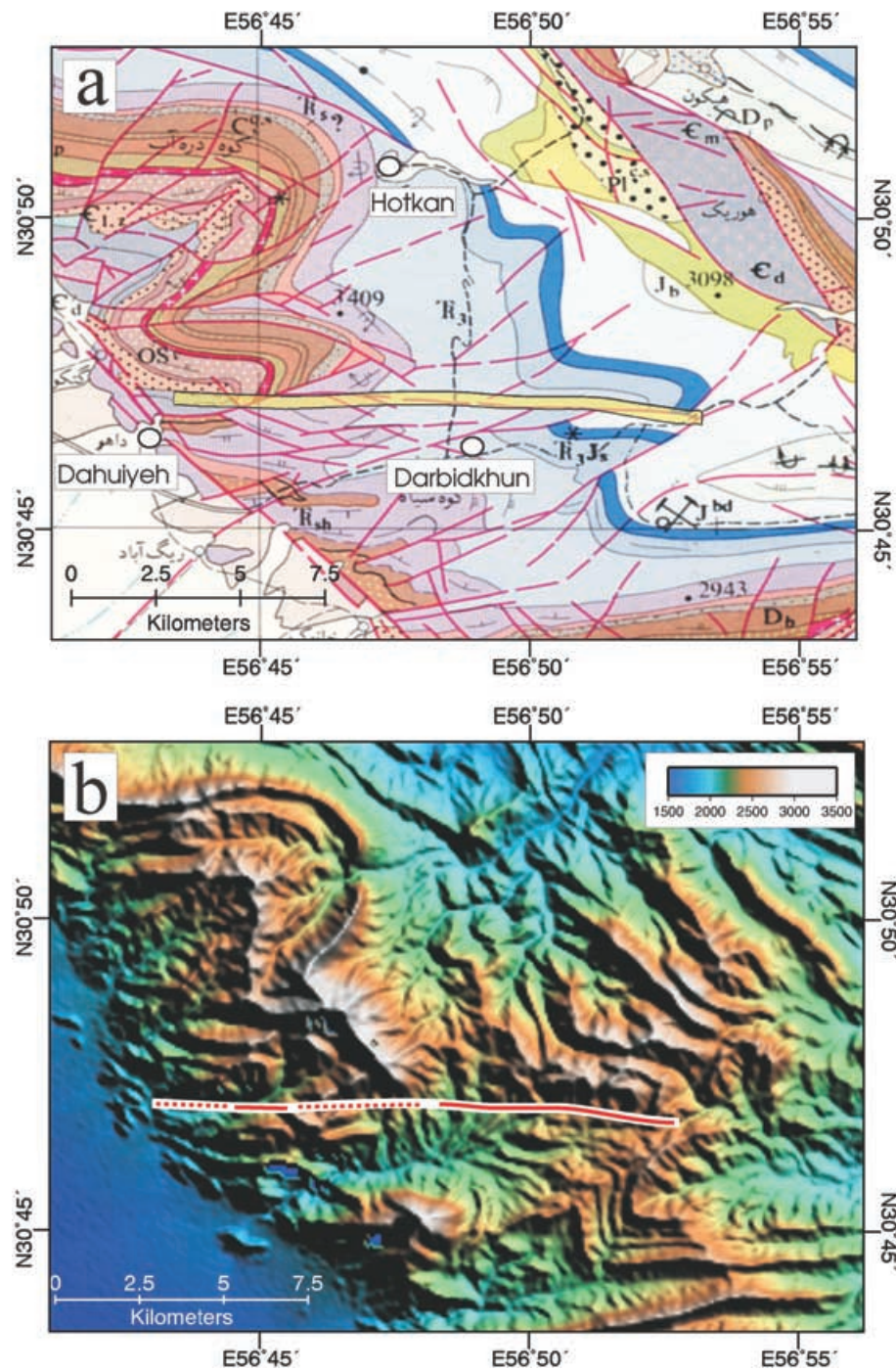


**Figure 2.** (a) Detail adapted from the Geological Survey of Iran map, 1:250 000 scale, for Rafsanjan (GSI 1992). The coseismic rupture in the 2005 Dahuiyeh earthquake follows the highlighted yellow line, which can be seen to follow a geological fault marked on the map (red line). Dashed black lines are roads. C is Cambrian, OS is Ordovician–Silurian, D is Devonian, TR is Triassic and J is Jurassic. (b) Shaded topography from the SRTM 90 m data set of the same region. The coseismic rupture in the 2005 Dahuiyeh earthquake is marked by the red line, continuous where observed as a scarp in the field and dotted where we infer the rupture to have been blind and not to have broken the surface (see text). (c) Detail from a LANDSAT TM scene of the same area. The 2005 coseismic rupture is marked as in (b) above. The red circle is the 2005 epicentre given in Table 1. The white arrows mark the NE–SW fault at the eastern end of the 2005 coseismic ruptures, referred to in the text.

### 3.2 Teleseismic bodywave modelling

The 2005 earthquake was widely recorded by stations of the Global Digital Seismic Network (GDSN), and the fault parameters of its centroid are well determined by long-period *P* and *SH* body waves. We first convolved the digital broad-band records from stations in the

teleseismic distance range of 30°–90° with a filter that reproduces the bandwidth of the old WWSSN 15–100 long-period instruments. At these wavelengths the source appears as a point source in space (the centroid) with a finite rupture time, and the resulting seismograms are sensitive to the source parameters of the centroid while relatively insensitive to the details of geological structure. We then used the

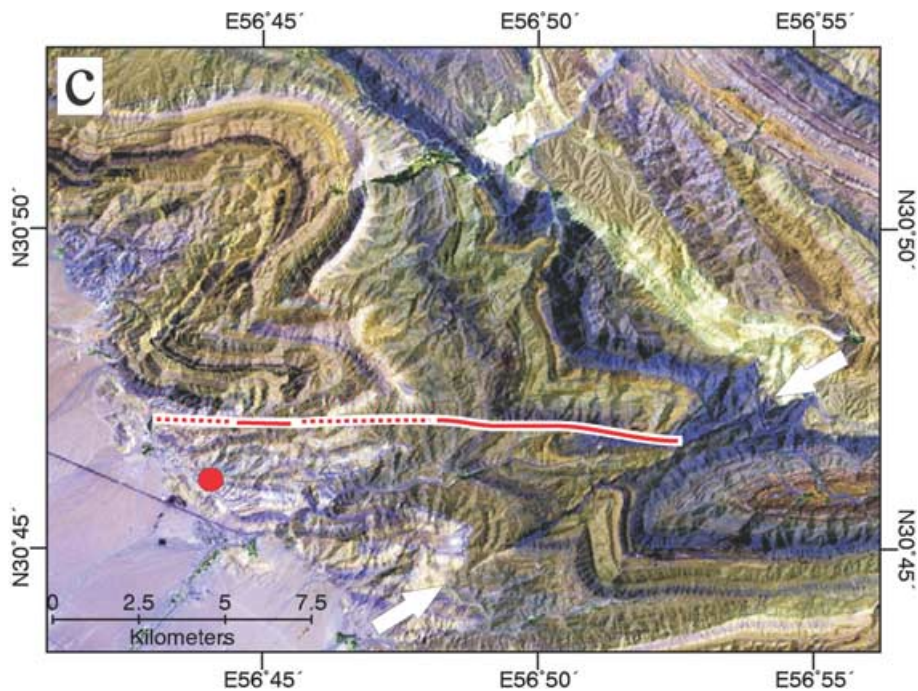


Figure 2. (Continued.)

**Table 1.** Summary of epicentral and source parameters for the earthquakes shown in Fig. 1. Latitude, longitude and origin time are from the relocations of Engdahl *et al.* (1998) or subsequent updates to their catalogue. Centroid depth (km), moment, strike, dip and rake are all determined from long-period *P* and *SH* waveforms using the method described here (Fig. 3). The last column lists the reference for waveform analysis: B93 is Baker (1993); B01 is Berberian *et al.* (2001); T04 is Talebian *et al.* (2004).

Date	Time	Lat.	Long.	Depth	Moment (N m)	$M_w$	Strike	Dip	Rake	Ref.
1977 December 19	23:34:33.0	30.911	56.413	7	$6.6 \times 10^{17}$	5.8	58	82	36	B93
1981 June 11	07:24:24.8	29.858	57.686	20	$9.5 \times 10^{18}$	6.6	169	52	156	B01
1981 July 28	17:22:24.1	29.976	57.767	18	$3.7 \times 10^{19}$	7.0	177	69	184	B01
1984 August 6	11:14:35.1	30.801	57.171	11	$1.1 \times 10^{17}$	5.3	279	35	86	B93
1998 Mar 14	19:40:29.6	30.126	57.585	5	$9.1 \times 10^{18}$	6.6	156	54	195	B01
2003 December 26	01:56:54.0	28.953	58.267	6	$7.6 \times 10^{18}$	6.5	357	88	194	T04
2005 February 22	02:25:22.1	30.774	56.736	7	$4.8 \times 10^{18}$	6.4	270	60	104	here

MT5 version (Zwick *et al.* 1994) of McCaffrey & Abers's (1988) and McCaffrey *et al.*'s (1991) algorithm, which inverts the *P* and *SH* waveform data to obtain the strike, dip, rake, centroid depth, seismic moment and the source time function (STF), which is parametrized by a series of isosceles triangle elements of half-duration  $\tau$  s. We always constrained the source to be a double couple. The method and approach we used are described in detail elsewhere (e.g. Nábělek 1984; McCaffrey & Nábělek 1987; Molnar & Lyon-Caen 1989; Taymaz *et al.* 1991) and are too routine to justify detailed repetition here.

The observed and synthetic seismograms for the 'best' minimum-misfit source parameters found by the inversion process are shown in Fig. 3. Nodal planes for both *P* and *SH* are well determined by the wide azimuth distribution of the recording stations, and the waveforms show a relatively simple pulse, typical of a shallow reverse-faulting earthquake, with STF of 7–9 s duration. It is clear from the surface and InSAR observations that the nodal plane dipping north is the fault plane, which has a strike of  $270^\circ$ , a dip of  $60^\circ$  and a rake of  $104^\circ$ . The centroid depth is 7 km and the moment is  $4.8 \times 10^{18}$  N m ( $M_w$  6.4). To investigate the uncertainties in these parameters, we carried out a number of tests, in which the parameter under investigation was held fixed at various values either side of

the 'best-fit' value, while the other parameters we allowed to vary, to minimize the misfit. In this way, we were able to see how much the parameters can be changed before there is a substantial deterioration in the fit between observed and synthetic seismograms. This, too, is now a routine procedure (see Molnar & Lyon-Caen 1989; Taymaz *et al.* 1991). We estimate the uncertainties to be  $\pm 10^\circ$  in strike,  $\pm 5^\circ$  in dip,  $\pm 15^\circ$  in rake,  $\pm 3$  km in depth and  $\pm 20$  per cent in moment.

Baker (1993), using the same method and procedure on digitized *P* and *SH* waves of the old WWSSN network, investigated the 1984 August 6 Hur earthquake, 10–15 km to the east of the 2005 Dahuiyeh event. The mechanism he obtained is shown in Table 1, and is similar in orientation (though with a somewhat shallower dip to the north-dipping nodal plane) and depth to that of the 2005 earthquake, though it was less widely recorded, with correspondingly larger errors estimated for strike ( $\pm 25^\circ$ ) and dip ( $\pm 10^\circ$ ), though similar errors in rake and depth.

### 3.3 Surface faulting, geological structure and geomorphology

The 2005 earthquake produced a series of coseismic ground ruptures running E–W over a distance of  $\sim 13$  km. Within a few hours of the

## 22 February 2005 Dahuiyeh 270/60/104/7/4.83E18

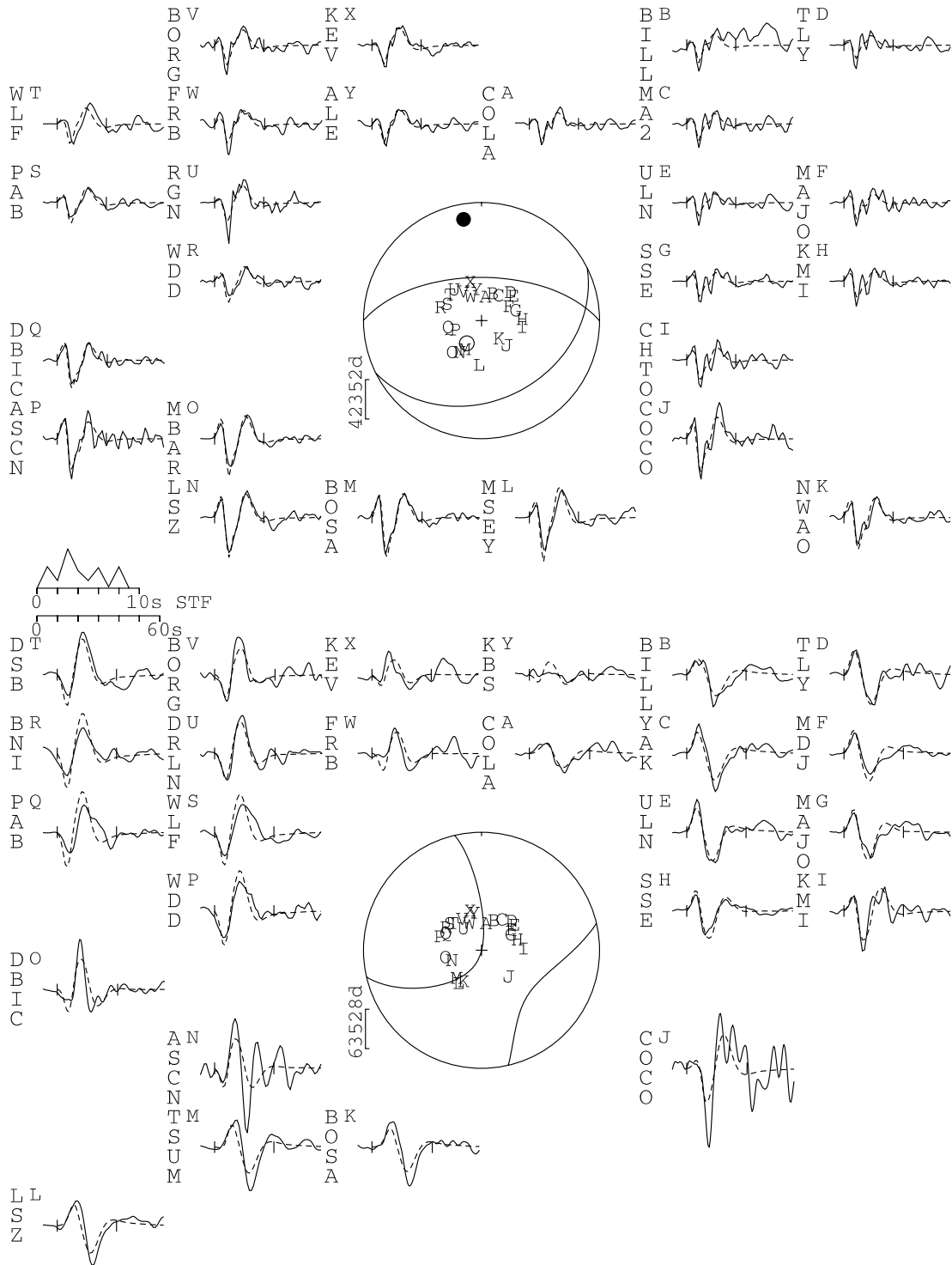


**Figure 3.** *P* and *SH* waveforms for 2005 February 22 Dahuiyeh earthquake. The event header shows the strike, dip, rake, centroid depth and scalar seismic moment (in N m) of the minimum misfit solution. The top focal sphere shows the lower hemisphere stereographic projection of the *P* waveform nodal planes, and the positions of the seismic stations used in the modelling routine. The lower focal sphere shows the *SH* nodal planes. Capital letters next to the station codes correspond to the position on the focal sphere. These are ordered clockwise by azimuth, starting at north. The solid lines are the observed waveforms, and the dashed lines are the synthetics. The inversion window is marked by vertical lines on each waveform. The source time function (STF) is shown, along with the timescale for the waveforms. The amplitude scales for the waveforms are shown below each focal sphere. The *P* and *T* axes within the *P* waveform focal sphere are shown by a solid and an open circle respectively.



**Figure 4.** (a) View north of the coseismic rupture cutting the Darbidkhun-Hotkan road (see Fig. 2a) at  $30^{\circ}46.993'N$   $56^{\circ}49.075'E$ . This picture was taken 1 day after the earthquake, by which time the scarp had been smoothed by bulldozer. The vertical offset is 105 cm. (b) View S from the air of the same locality as (a) on the eastern side of the road, showing a series of parallel open fissures caused by the collapse of the overhanging hanging wall.

earthquake, the part of these ruptures that crossed the road between Darbidkhun and Hotkan (Fig. 2a) had been noticed (Fig. 4). In this locality the scarp that formed was about 105 cm high, upthrown to the north (Fig. 4a). In general, it was associated with a series of parallel open fissures on the upthrown side (Fig. 4b), representing the collapse of the hanging wall. The scarp formed in well-bedded Triassic–Jurassic shales and sandstones, with a uniform orientation of strike  $280^{\circ}$  and dip  $70^{\circ}N$ ; essentially parallel to the orientation of the fault plane determined from the teleseismic waveform modelling. In this place, it was clear that the fault surface was parallel to the bedding, at least close to the surface.

Over the next 2 days, the surface rupture was followed in the field, and it became clear that the scarp at the road (Fig. 4) was part of a continuous E–W rupture that could be traced for 7 km westward from its eastern termination at  $30^{\circ}46.737'N$   $56^{\circ}52.469'E$ . Throughout this section, the fault was parallel to the bedding in the Triassic–Jurassic sediments, which varied very little, typically with a dip of  $60^{\circ}$ – $70^{\circ}N$ . The scarp itself approximately followed the south-facing base of an E–W ridge (Fig. 2b). Occasionally it crossed the north-facing slope of a side gully, reversing the local slope (Fig. 5a), and in several places it crossed incised streams (Fig. 5d), in which the northward dip of the fault was clearly visible. The general morphology of the scarp revealed that the overhanging hanging wall had collapsed to leave an open fissure (Fig. 5b), sometimes several metres behind where the reverse fault itself reached the surface (Fig. 5c).

Two characteristics of this continuous fault rupture are noteworthy. Firstly, it followed precisely a known fault within the Triassic–Jurassic succession, that was marked on the existing geological maps (Geological Survey of Iran 1992, 1995). The orientation of this pre-existing fault, and its association with the surrounding folding and geological structure, suggest that it originated with an earlier, pre-Late-Cenozoic phase of deformation, perhaps with a different slip vector, and with a substantial offset. Secondly, there was very little evidence in the local geomorphology for previous recent movement on this fault. Only at one place ( $30^{\circ}46.72'N$   $56^{\circ}5.18'E$ ), where the rupture crossed an incised N–S flowing stream, was there a hint of an earlier uplifted stream terrace that ended at the fault scarp; but even this was equivocal. The reason for this lack of evidence for earlier earthquake-generated scarps is probably because the topography is steep, the rocks are weak, easily eroded shales and sandstones, and

the winter rain and snow-melt are capable of removing such scarps quickly. This fault would have been very difficult to identify as active before the earthquake occurred.

The eastern limit of this continuous fault trace coincided with known geological fault striking NE–SW, that is clearly visible in the topography, satellite image and on the geological map (marked by white arrows in Fig. 2c). To the SE of this oblique fault, the Triassic–Jurassic rocks form a large fold with a steeply plunging axis, and bedding becomes strongly oblique to the coseismic rupture surface. The main road continues east, and crosses the projected line of the fault in several places, but showed no sign of surface rupture.

At the western end of the continuous trace ( $30^{\circ}47.098'N$   $56^{\circ}48.478'E$ ), the projected fault again enters a region where the Triassic–Jurassic rocks are severely contorted into a series of folds with almost-vertical axes. A thorough search in this area failed to find evidence of surface rupture, until a point  $\sim 5.5$  km west of the end of the continuous trace, at  $30^{\circ}47.027'N$   $56^{\circ}45.082'E$ , where a convincing linear scarp about 300 m long was found (Figs 2, 5e and f). At this place the scarp is in Triassic limestones and runs along a north-facing slope of an E–W valley, thus reversing the local slope with its upward throw to the north of  $\sim 100$  cm. The location of this scarp, precisely along-strike from that in the west, and its sense of throw in the opposite sense to the local slope, make its coseismic tectonic origin very likely. As we show in the next section, that interpretation is also consistent with the InSAR interpretation. The scarp in Figs 5(e) and (f) runs westward into the bottom of a major E–W river valley, which itself follows the trace of a known geological fault. On its north side are lower Cambrian (Desu Formation) red beds with abundant gypsum, striking  $090^{\circ}$  and dipping uniformly  $45^{\circ}N$ . On the south side are limestones and shales of Devonian age with quite variable dips, generally towards the south at  $\sim 45^{\circ}$ . In the next section we show it is very likely that the coseismic rupture followed the geological fault in the river bed, and was thus subparallel to the bedding in the Cambrian rocks on the north side. Although we found evidence for some bedding-plane slip in those Cambrian rocks near the valley floor, we found no evidence of a continuous fault trace in the valley floor itself.

In summary, the observed surface ruptures have several important characteristics. They were observed only where the local

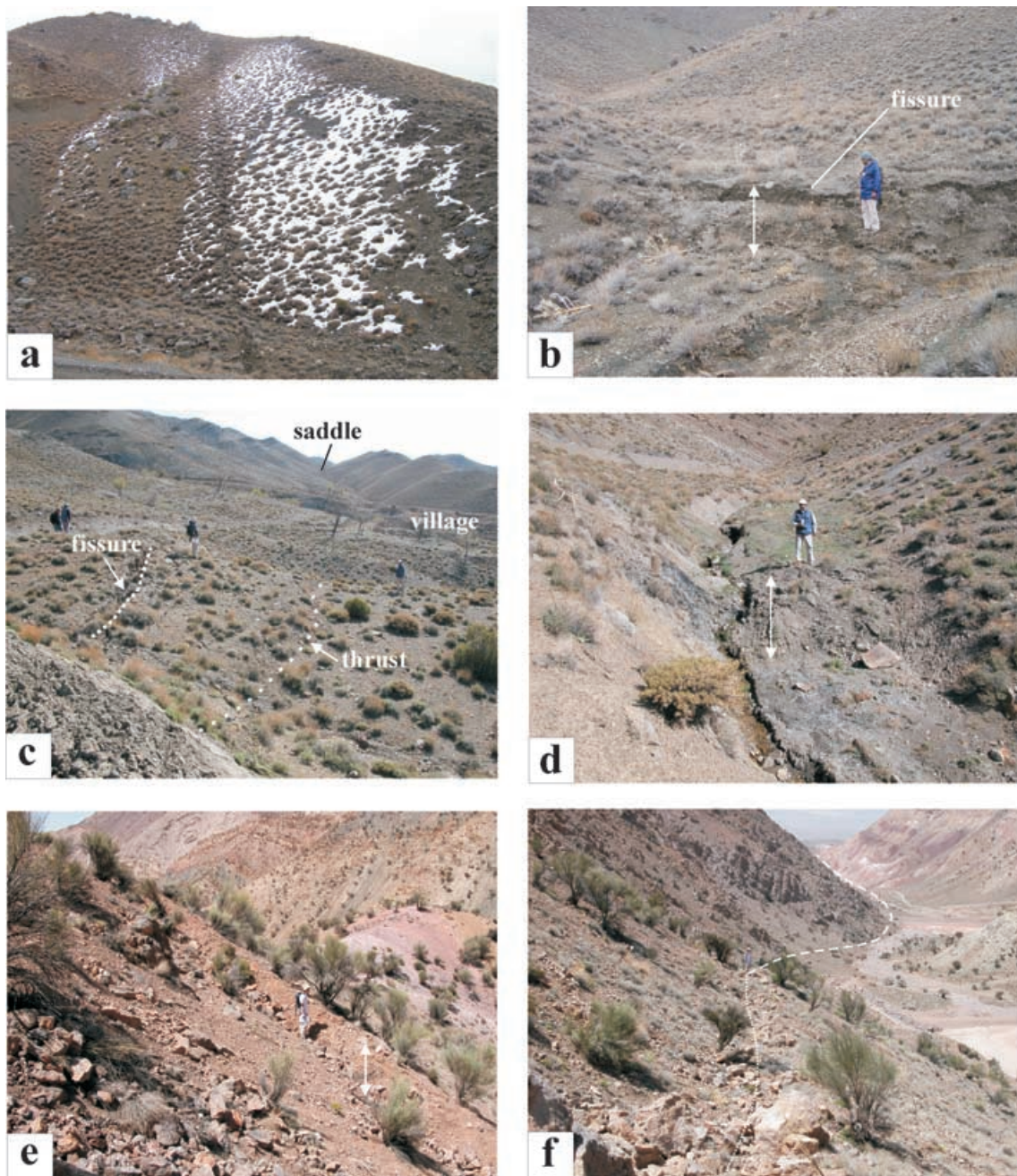


**Figure 5.** Field photos of the surface ruptures in the 2005 Dahuiyeh earthquake. (a) View east along the scarp at  $30^{\circ}46.819'N$   $56^{\circ}51.667'E$ , where the fault crosses a dirt track (foreground), then a stream and runs up a snow-covered north-facing slope. The fault is upthrown  $\sim 60$  cm on the north (left), thus reversing the local snow-covered slope. (b) View north of the scarp where it crosses a minor stream at  $30^{\circ}46.838'N$   $56^{\circ}51.520'E$ . The overhanging hanging wall has collapsed to form a vertical open fissure. The vertical offset (white arrow) is  $\sim 100$  cm. (c) View east where the scarp runs behind an abandoned village at  $30^{\circ}46.950'N$   $56^{\circ}49.505'E$ , with vertical offset  $\sim 50$  cm. Again, the hanging wall has collapsed to leave a vertical fissure. The fault continues east to through the saddle in the skyline. (d) View north of the fault crossing a gully at  $30^{\circ}46.959'N$   $56^{\circ}49.642'E$ , with vertical offset (white arrow)  $\sim 60$  cm. Here the fault is clearly parallel to the bedding in the Triassic–Jurassic sandstones and shales, and dips at  $60^{\circ}N$ . (e) View NW of the fault at  $30^{\circ}47.027'N$   $56^{\circ}45.082'E$ . The vertical offset (white arrow) is  $\sim 100$  cm, up on the north (right) side, thus reversing the local slope. The person is standing at the foot of the scarp. (f) View west about 50 m west of (e), showing the scarp (dotted line) offsetting the local slope with the downhill side upthrown. The fault descends the slope to the valley, where we infer it continued along the line of the river (dashed line), which is a reverse fault dipping N (right). The red rocks dipping N in the background are the Cambrian rocks of the Desu Formation.

bedding was uniform, planar and subparallel to the orientation of the rupture plane determined seismologically. In those places, the rupture surface clearly followed the bedding, at least near the surface. The InSAR data discussed below show that the rupture almost certainly extended at depth over the entire distance from its easternmost

surface expression to Kuh Banan fault in the west. However, where the rocks at the surface were folded, with bedding oblique to the rupture plane, then the fault was 'blind', and did not reach the surface itself. In those places the surface expression of the fault was presumably coseismic warping or folding.

**Table 2.** Summary of Envisat data used to produce interferograms. The incidence angle is measured relative to the vertical. The first image of each pair was acquired on Date 1, and the second on Date 2, separated by  $\Delta t$  days. The perpendicular baseline between the orbits in each pass is  $B_{\perp}$  m.

	Track	Incidence angle	Azimuth	Date 1	Date 2	$\Delta t$ (days)	$B_{\perp}$ (m)
Ascending	285	41°	349.2°	2004/09/19	2005/03/13	175	75
Descending	435	23°	190.7°	2005/02/17	2005/03/24	35	61

### 3.4 SAR Interferometry

We used Envisat ASAR data and the JPL/Caltech ROI\_PAC software (Rosen *et al.* 2004) to construct two interferograms spanning the earthquake, one from an ascending track in acquisition mode IS6 (centre-scene incidence angle 41°), and one from a descending track in the more usual IS2 mode (incidence angle 23°). Precise orbits provided by ESA were used but no further orbital adjustments were made. The topographic phase contribution was removed using the three-arcsec (90 m) SRTM DEM (with voids left unfilled) and the interferograms cleaned using a power spectrum filter (Goldstein & Werner 1998). Acquisition data are given in Table 2 and the observed wrapped interferograms are shown in Figs 6(a) and (b).

Perpendicular baselines are small ( $\leq 75$  m) and the correlation is generally good for both interferograms, with the exception of a few areas. The ascending track interferogram, which spans the whole winter, suffers from temporal decorrelation in a band crossing the SW of the interferogram (corresponding to a vegetated area of the Zarand plain) and in patches over high ground in the NW (most likely due to snow). However, the most significant decorrelation, which is present in both interferograms, is an  $\sim 18 \times 8$  km patch close to the faulting itself. This decorrelation is partly a result of the steep terrain, and possibly snow, in this mountainous area. However, some other steep, elevated parts of the interferograms are coherent and so coseismic ground shaking and land sliding are probably also contributing factors.

Maximum line-of-sight displacements are  $\sim 20$  cm (7 fringes) towards the satellite and  $\sim 20$  cm away from the satellite for the ascending interferogram, and  $\sim 40$  cm (14 fringes) towards and  $\sim 45$  cm (16 fringes) away from the satellite for the descending interferogram. The area to the north of the central decorrelated patch shows displacements towards the satellite in both interferograms, and the area south of the patch shows displacements away from the satellite in both interferograms. The ascending interferogram has an eastward pointing line-of-sight vector, while the descending interferogram has a westward pointing line-of-sight vector; E–W motions would, therefore, cause oppositely signed displacements in one interferogram compared to the other. Since this is not the case, it follows that the line-of-sight displacements are dominated by vertical motions. This in turn helps explain why the descending interferogram contains more fringes than the ascending one: with its steeper incidence angle, the descending interferogram is more sensitive to vertical motions. Taken together, the interferograms are therefore consistent with uplift on the north side of a roughly E–W fault, and subsidence to the south of it.

In spite of the decorrelated central region, it is clear from both interferogram pairs that the northern and southern fringe lobes join at points close to the west and east ends of the observed surface ruptures (black dots). This in turn indicates that the causative fault is of similar length to the ruptures observed in the field. In the ascending interferogram, there are also fringes showing negative line-of-sight displacement at 30°49'N 56°32'E. These correspond with a vegetated area in the town of Zarand and we suspect it to

be the result of subsidence, perhaps due to ground-water pumping, during the  $\sim 6$  month period spanned by the interferogram. This feature is absent from the descending interferogram, presumably because of its much shorter (35 days) timespan.

To model the interferometric data, we first resampled the interferograms using a quadtree algorithm (e.g. Jonsson *et al.* 2002), reducing them from  $\sim 2$ – $3$  million to  $\sim 1000$  points each. We then inverted these data using a downhill simplex algorithm with Monte-Carlo restarts (Wright *et al.* 1999), to solve for uniform slip on a single, rectangular fault in an elastic half-space (Okada 1985). The fault location, length and top and bottom depths, strike, dip, rake, and slip, were all free to vary in the inversion.

The best-fit solution (Table 3, Figs 6c and d) shows almost pure reverse faulting on a steep, north-dipping fault plane extending from 9.6 km depth to the surface. Errors were estimated by inverting 100 data sets perturbed by realistic correlated noise (Wright *et al.* 2005). The best-fit parameters are close to those of the focal mechanism obtained by *P* and *SH*-waveform inversion (the equivalent ‘centroid depth’ for the InSAR model is  $\sim 4.7$  km), and differences in the orientation between the two are within the allowable errors in the two inversions.

The simple one-fault model fits the data well to a first order (Figs 6e and f), especially in the eastern part of the fault zone. The calculated fault does not project to the surface at precisely the locations where surface ruptures were observed in the field (Figs 6c and d), though the disagreement is everywhere less than 0.6 km. Since the field observations indicate that the fault reached the surface by following bedding planes, where they happened to be favourably oriented locally, we doubt whether the disagreement is significant. Nonetheless, residuals in Figs 6(e) and (f) include three fringes west of the modelled fault (for the ascending track), and the same number to the south and north of the fault (for the descending track). A kinked fault, with a change in strike at some point along its length, might account for some of these residual fringes, but such an elaboration cannot at present be directly supported by field evidence.

In conclusion, a consistent first-order picture of coseismic rupture surface is revealed by the seismology, InSAR and field data. The best-fit solutions of the seismological and InSAR models differ significantly only for moment, the InSAR estimate being 38 per cent higher than the seismological estimate. The assumption of uniform slip in the InSAR model may account for some of this difference. Another possibility is that since the second pass of the interferogram pairs was 2 weeks and 1 month after the earthquake, the InSAR analysis involves some afterslip. Using the fault length of 12.6 km based on InSAR, the seismic moment and centroid depth yield an average slip of 0.8 m, compared with the 1.6 m from the InSAR model.

## 4 DAMAGE, CASUALTIES AND EPICENTRAL LOCATION

The two villages most affected by the 2005 earthquake were Dahuiyeh, at the western end of the coseismic surface faulting, and Hotkan, about 7 km north of the central part of the fault ruptures

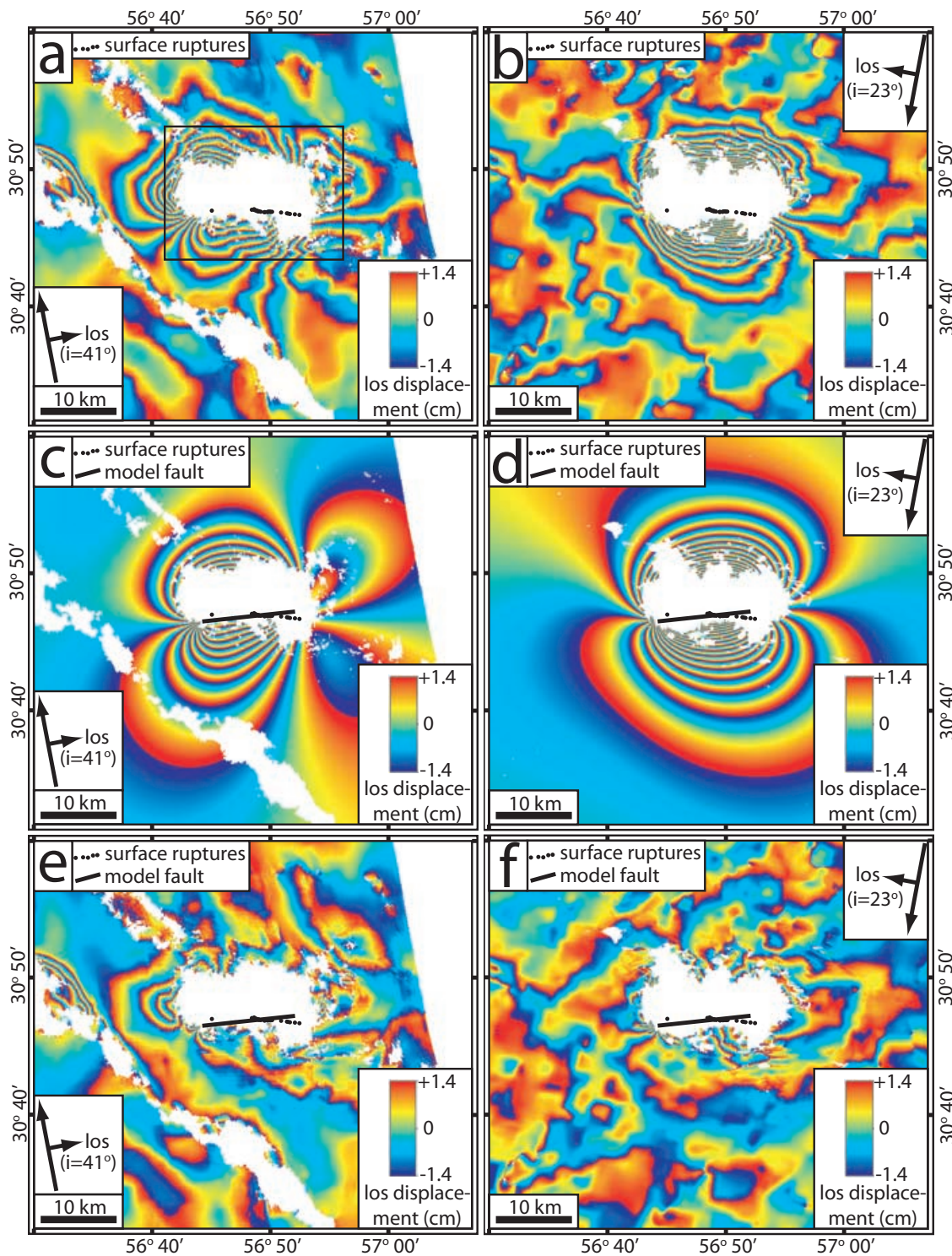


**Figure 6.** Radar interferograms, in all cases shown wrapped, with one fringe representing a 28 mm line-of-sight change between the ground and the satellite (see Table 2 for acquisition parameters). In each case the inset with arrows shows the satellite track and line-of-sight (los) directions, with inclination to the downward vertical ( $i$ ) in degrees. White areas are incoherent. (a) ascending and (b) descending radar interferograms. The black box in (a) marks the area covered in Fig. 2. The positions of the observed coseismic surface ruptures are marked by the line of black dots in the decorrelated area in the middle of the fringe patterns. (c) and (d) are synthetic interferograms calculated for the ascending (c) and descending (d) orbits, using the fault parameters in Table 3. The thin solid line is the projection to the surface of the fault used to calculate the synthetics. (e) and (f) are the residuals left by subtracting observed and synthetic interferograms in the ascending (e) and descending (f) cases.

**Table 3.** Fault plane parameters from the inversion of interferometric and seismic data. The average slip for the seismological solution is calculated assuming the fault length of 12.5 km from the InSAR analysis, and the centroid depth of 7 km (i.e. total fault depth of 14 km). The depth of the seismological model is the centroid depth, whereas in the InSAR model the depth is to the base of the fault.

Data inverted	Strike	Dip	Rake	Slip	Depth	Length	Moment (N m)
InSAR interferograms	$266 \pm 1^\circ$	$67 \pm 2^\circ$	$105 \pm 2^\circ$	$1.7 \pm 0.1$ m	$9.3 \pm 0.3$ km	$12.5 \pm 0.2$ km	$6.7 \pm 0.2 \times 10^{18}$
<i>P</i> and <i>SH</i> body waves	$270 \pm 10^\circ$	$60 \pm 5^\circ$	$104 \pm 5^\circ$	(0.8 m)	( $7.0 \pm 3$ km)	–	$4.9 \pm 1.0 \times 10^{18}$



**Figure 7.** (a) View west over Dahuiyeh. Old Dahuiyeh is almost totally destroyed in the foreground. In the background, on the Zarand plain, is the more modern settlement of new Dahuiyeh, resettled before the earthquake and considerably less damaged. (b) View west along the ridge of Hotkan. The village is completely destroyed, with hardly a building left standing. Only a few door and window frames remain identifiable.

(Fig. 2a). About 150 and 300 people were killed in each place, respectively. Some damage was sustained by other villages along the Kuh Banan range front, but the mountainous region to the east is relatively sparsely inhabited. The small hamlet of Darbidkhun (Fig. 2a) suffered considerable damage, but with few casualties. The old village of Dahuiyeh, situated at the range front, was largely constructed from traditional sun-dried mud brick, and was almost totally destroyed, with only a few modern buildings surviving without collapse (Fig. 7a). Casualties would have been far worse, had not the majority of the population already moved to a new location a few km west in the Zarand plain, before the earthquake. The new Dahuiyeh is constructed largely of modern materials, and relatively few buildings collapsed.

Hotkan is situated on a high ridge above a fertile valley in the mountains, and was completely destroyed (Fig. 7b), with hardly any buildings surviving. Construction was largely of stone-rubble walls, which collapsed, failing to support heavy roofs of timber covered with clay.

There is some interest in the damage distribution from the perspective of epicentral location error. The best current instrumental epicentre location, courtesy of R. Engdahl (personal communication, 2005 June 13) and based largely on arrival time data at regional-distance stations in Iran, is close to Dahuiyeh, just south of the observed line of surface ruptures (Fig. 1b; Table 1). The true epicentre must lie north of this line. If the fault has a constant dip of  $60^\circ$ N, it projects to a depth of  $\sim 12$  km beneath Hotkan, which is close to the base of the fault inferred from InSAR data (Table 3). If, as is often the case (Mori *et al.* 1995), the earthquake nucleated near the base of the seismogenic zone, we would expect the epicentre to have a latitude rather similar to that of Hotkan, that is, to be shifted about 5–10 km north of that in Table 1 and Fig. 1(b).

## 5 DISCUSSION

In one respect, the fact that the fault responsible for the 2005 Dahuiyeh earthquake was a reverse fault is unremarkable. The principal style of deformation within Iran is shortening, to accommodate convergence between Arabia and Eurasia, and reverse-faulting earthquakes are common. However, the association of the 2005 earthquake fault with the adjacent Kuh Banan strike-slip fault is worth considering, because the 2005 earthquake reverse fault was within the mountains at a high angle to the range front, and not along the range front itself, which is a far more common occurrence.

Large intracontinental strike-slip faults, such as the Kuh Banan fault, differ from transform faults in the oceans, in that they seem to end, or terminate, rather than simply connect with another part of a continuous plate boundary. Much recent attention has been directed towards these terminations, which in many cases involve the strike-slip fault ending in a dip-slip fault with an oblique trend, whose displacement dies away with distance from the end of the strike-slip fault. Examples have been described from Mongolia (Bayasgalan *et al.* 1999), northern Tibet (Meyer *et al.* 1998) and Iran (Berberian *et al.* 2000), all of which involve reverse-fault terminations, and from Greece (Goldsworthy *et al.* 2002), where the strike-slip faults end in normal faulting. In all these places, the function of these dip-slip faults is probably to allow the strike-slip fault to terminate in rotations about a vertical axis.

In the context above, the oblique angle between the 2005 Dahuiyeh earthquake rupture and the Kuh Banan strike-slip fault, looks familiar. However, it is not likely that the Kuh Banan fault actually terminates in the south at Dahuiyeh. The range front continues another 15 km to the south, though with less geomorphological evidence for recent faulting than farther north, to the latitude of

Gorchuiyeh (Fig. 1b), where it then bends east into what is clearly a thrust or reverse fault, with uplifted and abandoned modern fan surfaces indicating recent movement. The Dahuiyeh earthquake reverse fault seems to be a splay coming off the Kuh Banan fault before its actual termination. This behaviour has also been observed elsewhere, and a good example is the faulting associated with the great Gobi-Altai earthquake ( $M_w \sim 8$ ), described by Baljinyam *et al.* (1993) and Bayasgalan *et al.* (1999) and summarized in Fig. 8. The main coseismic rupture in 1957 involved left-lateral strike-slip along the ranges of Ih Bogd and Baga Bogd, but coseismic reverse (or thrust) faulting was also observed at Toromhon and at the eastern end of Baga Bogd. The Toromhon fault was a substantial thrust (or reverse) fault splaying off the main left-lateral faulting and clearly absorbed some of the strike-slip offset, which was greater west of Toromhon and smaller to the east. Both Toromhon and Baga Bogd reverse faults died out to the south, and so does the reverse fault at the east end of Arts Bogd, which did not rupture in 1957. The situation at the southern end of Kuh Banan is rather similar (Fig. 8). If the Dahuiyeh reverse fault absorbs some of the strike-slip motion, that may account for why the Kuh Banan range front shows less clear evidence for Holocene offsets between Dahuiyeh and Gorchuiyeh. Other than the observation that the 2005 coseismic ruptures did not continue east of the oblique structure marked by white arrows in Fig. 2(c), we have no evidence that the displacement on the 2005 Dahuiyeh reverse fault decreases away from the Kuh Banan fault. It is also unclear whether the 1986 Hur earthquake, further to the east (Fig. 1b) was on the same, or a related, structure at depth.

Thus the 2005 earthquake fault may have a tectonic function that is understandable, at least in principle. However, the fault has a brutal lesson to teach in terms of seismic hazard assessment, as such intramountain reverse faults are much more difficult to assess as active than the ones that bound range fronts. Reverse fault splays at an oblique angle to strike-slip faults are common in Iran (e.g. Walker & Jackson 2004), and many are marked on geological maps. We suspect that, like the 2005 Dahuiyeh earthquake fault, their location within the mountains, where erosion and land sliding remove traces

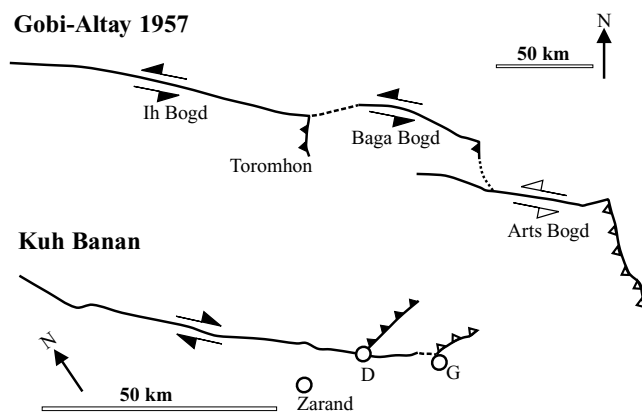


**Figure 8.** A comparison between the fault pattern in the region of the 1957 Gobi-Altai earthquake ( $M_w \sim 8$ ) in Mongolia (top) and the Kuh Banan and Dahuiyeh system of faults in Iran (bottom). Note the different scales. For ease of comparison, the two fault systems are drawn parallel: in fact the Gobi-Altai fault trends E–W, while the Kuh Banan fault trends NNW–SSE. The 1957 ruptures in Mongolia followed the northern sides of Ih Bogd and Baga Bogd mountains, ending in reverse faults that also moved (black triangles) at the eastern end of each segment. The Arts Bogd segment, which also ends in a reverse fault (white triangles) did not move in 1957. The 2005 Dahuiyeh (D) reverse fault is marked by black triangles, and the reverse fault at Gorchuiyeh (G) is marked by white triangles.

of recent activity, and the unlikelihood of them cutting large areas of Quaternary deposits, may make their seismic potential difficult to assess and easy to miss.

## 6 CONCLUSIONS

From the seismotectonic and seismic hazard points of view, the important feature of the 2005 Dahuiyeh earthquake was that it occurred on an intramountain reverse fault. Most reverse-faulting earthquakes in Iran occur on faults that bound the range fronts, and are easily recognizable in the geomorphology. By contrast, the 2005 earthquake occurred on a fault which, although known and mapped in the geology, could not reasonably have been identified as active beforehand, as any signs of its previous seismogenic activity had been obscured by weathering and land sliding. Other intramountain reverse fault earthquakes are known to have occurred in Iran before, such as the 1984 Hur earthquake nearby, but the 2005 event was the first we know of that produced a clear, mapped surface rupture, and could also be studied by InSAR. The 2005 earthquake fault occurred close to the Kuh Banan strike-slip fault, which follows a range front, but at an oblique angle to it, and has several characteristics of reverse fault splays that come off other strike-slip faults, both in Iran and elsewhere. These reverse fault splays are probably related to the way the strike-slip faults terminate, and may indicate rotations about vertical axes.

## ACKNOWLEDGMENTS

We thank Manuel Berberian for information about the 1984 Hur earthquake, Bob Engdahl for quickly making available his recalculated epicentre for the 2005 Dahuiyeh earthquake and Brian Emmerson for help with the seismic data. We are grateful to E. Fielding and V. Regard for constructive reviews. We thank M. T. Korehei, M. Ghassemi and M. Hoseini for providing the facilities and support of the Geological Survey of Iran, and A. Rashidi for help in the field. This work was supported by an NERC grant to COMET (<http://comet.nerc.ac.uk>). Cambridge Earth Sciences contribution 8251.

## REFERENCES

- Ambraseys, N.N. & Melville, C.P., 1982. *A history of Persian earthquakes*, Cambridge University Press, UK, p. 219.
- Baker, C., 1993. The active seismicity and tectonics of Iran, *PhD thesis*, (unpublished), University of Cambridge, p. 228.
- Baljinyam, I. *et al.*, 1993. Ruptures of major earthquakes and active deformation in Mongolia and its surroundings, *Geol. Soc. Am. Memoir*, **181**, p. 62.
- Bayasgalan, A., Jackson, J., Ritz, J.F. & Carretier, S., 1999. Field examples of strike-slip fault terminations in Mongolia, and their tectonic significance, *Tectonics*, **18**, 394–411.
- Berberian, M. & Yeats, R.S., 1999. Patterns of historical earthquakes rupture in the Iranian plateau, *Bull. seism. Soc. Am.*, **89**, 120–139.
- Berberian, M., Asudeh, I. & Arshadi, S., 1979. Surface rupture and mechanism of the Bob-Tangol (southeastern Iran) earthquake of 19 December 1977, *Earth planet. Sci. Lett.*, **42**, 456–462.
- Berberian, M., Jackson, J.A., Qorashi, M. & Kadjar, M.H., 1984. Field and teleseismic observations of the 1981 Golbaf-Sirch earthquakes in SE Iran, *Geophys. J. R. astr. Soc.*, **77**, 809–838.
- Berberian, M., Jackson, J.A., Qorashi, M., Talebian, M., Khatib, M.M. & Priestley, K., 2000. The 1994 Sefidabeh earthquakes in eastern Iran: blind thrusting and bedding-plane slip on a growing anticline, and active tectonics of the Sistan suture zone, *Geophys. J. Int.*, **142**, 283–299.
- Berberian, M. *et al.*, 2001. The March 14 1998 Fandoqa earthquake ( $M_w$  6.6) in Kerman province, SE Iran: re-rupture of the 1981 Sirch earthquake

fault, triggering of slip on adjacent thrusts, and the active tectonics of the Gowk fault zone, *Geophys. J. Int.*, **146**, 371–398.

Engdahl, E.R., van der Hilst, R. & Buland, R., 1998. Global teleseismic earthquake relocation with improved travel times and procedures for depth determination, *Bull. seism. Soc. Am.*, **3**, 722–743.

Geological Survey of Iran, 1992. Geological Map of Rafsanjan, 1:250,000 scale.

Geological Survey of Iran, 1995. Geological Map of Zarand, 1:100,000 scale.

Goldstein, R.M. & Werner, C.L., 1998. Radar interferogram filtering for geophysical applications, *Geophys. Res. Lett.*, **25**, 4035–4038.

Goldsworthy, M., Jackson, J. & Haines A.J., 2002. The continuity of active fault systems in Greece, *Geophys. J. Int.*, **148**, 596–618.

Jonsson, S., Zebker, H., Segall, P. & Amelung, F., 2002. Fault slip distribution of the  $M_w$  7.2 Hector mine earthquake estimated from satellite radar and GPS measurements, *Bull. seism. Soc. Am.*, **92**, 1377–1389.

McCaffrey, R. & Abers, J., 1988. *SYN3: a program for inversion of teleseismic body wave form on microcomputers*, Air Force Geophysical Laboratory Technical Report, AFGL-TR-88-0099, Hanscomb Air Force Base, Massachusetts.

McCaffrey, R. & Nábělek, J., 1987. Earthquakes, gravity, and the origin of the Bali Basin: an example of a nascent continental fold-and-thrust belt, *J. geophys. Res.*, **92**, 441–460.

McCaffrey, R., Zwick, P. & Abers, G., 1991, *SYN4 Program*, IASPEI Software Library, **3**, 81–166.

Meyer, B., Taponnier, P., Bourjot, L., Metivier, F., Gaudemer, Y., Peltzer, G., Shunmin, G. & Zhitai, C., 1998. Crustal thickening in Gansu-Qinghai, lithospheric mantle subduction, and oblique, strike-slip controlled growth of the Tibet plateau, *Geophys. J. Int.*, **135**, 1–47.

Molnar, P. & Lyon-Caen, H., 1989. Fault plane solutions of earthquakes and active tectonics of the Tibetan Plateau and its margin, *Geophys. J. Int.*, **99**, 123–153.

Mori, J., Wald, D.J. & Wesson, R.I., 1995. Overlapping fault planes of the 1971 San Fernando and 1994 Northridge, California earthquakes, *Geophys. Res. Lett.*, **22**, 1033–1036.

Nábělek, J., 1984. Determination of earthquake source parameters from inversion of body waves, *PhD thesis*, MIT, Cambridge, Massachusetts.

Okada, Y., 1985. Surface deformation due to shear and tensile faults in a half-space, *Bull. seism. Soc. Am.*, **75**, 1135–1154.

Rosen, P.A., Hensley, S., Peltzer, G. & Simons, M., 2004. Updated Repeat Orbit Interferometry package released. *EOS, Trans. Am. geophys. Un.*, **85**, 35.

Talebian, M. *et al.*, 2004. The 2003 Bam (Iran) earthquake: rupture of a blind strike-slip fault, *Geophys. Res. Lett.*, **31**, L11611.

Taymaz, T., Jackson, J. & McKenzie, D., 1991. Active tectonics of the north and central Aegean Sea, *Geophys. J. Int.*, **106**, 433–490.

Vernant, Ph. *et al.*, 2004. Contemporary crustal deformation and plate kinematics in Middle East constrained by GPS measurements in Iran and northern Oman, *Geophys. J. Int.*, **157**, 381–398.

Walker, R. & Jackson, J., 2002. Offset and evaluation of the Gowk Fault, S.E. Iran: a major intra-continental strike-slip system, *J. Struct. Geol.*, **24**, 1677–1698.

Walker, R. & Jackson, J., 2004. Active tectonics and Late Tertiary strain distribution in central and eastern Iran. *Tectonics*, **23**, TC5010.

Walker, R., Jackson, J. & Baker, C., 2003. Thrust faulting in eastern Iran: source parameters and surface deformation of the 1978 Tabas and 1968 Ferdows earthquake sequences, *Geophys. J. Int.*, **152**, 749–765.

Walker, R., Bergman, E., Jackson, J., Ghorashi, M. & Talebian, M., 2005. The 22 June 2002 Changureh (Avaj) earthquake in Qazvin province, NW Iran: epicentral re-location, source parameters, surface deformation and geomorphology, *Geophys. J. Int.*, **160**, 707–720.

Wright, T.J., Parsons, B.E., Jackson, J.A., Haynes, M., Fielding, E.J., England, P.C. & Clarke, P.J., 1999. Source parameters of the 1 October 1995 Dinar (Turkey) earthquake from SAR interferometry and seismic body-wave modelling, *Earth planet. Sci. Lett.*, **172**, 23–37.

Wright, T.J., Parsons, B.E. & Lu, Z., 2004. Towards mapping surface deformation in three dimensions using InSAR, *Geophys. Res. Lett.*, **31**, L01607.

Wright, T.J., Clarke, P. & Funning, G., 2005. Realistic errors for models derived from InSAR data, *J. geophys. Res.*, submitted.

Zwick, P., McCaffrey, R. & Abers, G., 1994, *MT5 Program*, IASPEI Software Library, **4**.

## APPENDIX

The 2005 surface ruptures occurred in high mountainous country in material that makes preservation of the scarps, even for a short time, extremely unlikely. We, therefore, include in this Appendix a list (Table A1) of the precise GPS-determined locations of some positions on the scarps that we visited in the field in 2005 February–April. This will enable anyone interested in visiting these locations, for example to carry out palaeoseismological trenching investigations, to find their exact position. The sites are listed in order, from east to west.

**Table A1.** GPS locations (in degrees, minutes, seconds) of sites visited on the 2005 coseismic fault scarps. The vertical offset on the scarp(s), where it could be estimated is given by  $V$ , in cm.

°	Longitude		°	Latitude		Comments
	'	"		'	"	
56	52	28.3	30	46	44.5	$V = 50$ cm, cuts old road in bend
56	52	05.2	30	46	47.1	$V = 40$ cm, cuts dirt track
56	51	40.4	30	46	48.6	$V = 60$ cm, cuts mining road and stream to east; possibly two terraces in the stream above the fault.
56	51	31.2	30	46	50.3	$V = 100$ cm
56	51	25.0	30	46	51.1	$V = 50$ cm, strike = 275, dip = 80°N
56	50	56.2	30	46	54.8	$V = 50$ cm, strike = 275
56	50	10.3	30	46	57.5	on slope down to a river
56	50	01.1	30	46	58.3	distributed cracking
56	50	06.6	30	46	57.4	$V = 40$ cm, on a saddle between valleys
56	50	04.0	30	46	57.1	$V = 30$ cm
56	49	58.9	30	46	57.9	$V = 30$ cm
56	49	53.4	30	46	58.0	$V = 30$ cm
56	49	51.2	30	46	58.1	$V = 30$ cm
56	49	46.4	30	46	57.1	next to abandoned village
56	49	34.3	30	46	57.1	$V = 60$ cm, crosses stream, dip = 60°N
56	49	31.9	30	46	56.7	$V = 40$ cm,
56	49	13.8	30	46	58.1	$V = 105$ cm, dip = 70, cuts tarmac road
56	49	04.8	30	46	58.9	Darbidkhun-Hotkan
56	49	03.6	30	46	59.8	
56	49	00.8	30	46	59.6	
56	48	58.5	30	47	00.5	$V = 80$ cm, cuts small stream
56	48	55.8	30	47	01.2	
56	48	52.9	30	47	01.8	$V = 100$ cm
56	48	49.5	30	47	03.9	50 cm wide fault zone
56	48	47.9	30	47	02.4	$V = 40+$ cm, strike = 280
56	48	43.2	30	47	04.8	50 cm wide fault zone, strike = 230, evidence of right-lateral offset
56	48	41.6	30	47	06.1	2 m wide fault zone, strike = 240
56	48	40.1	30	47	08.8	minor cracks
56	48	28.7	30	47	05.9	
56	45	04.9	30	47	01.6	$V = 100$ , in limestone, reversing local slope, strike = 260